# Stability and Bifurcations in Neural Fields with Axonal Delay and General Connectivity

Fatihcan M. Atay
Max Planck Institute for Mathematics in the Sciences,
Inselstr. 22, Leipzig 04103, Germany.
E-Mail: atay@member.ams.org

Axel Hutt*
Weierstrass Institute for Applied Analysis and Stochastics,
Mohrenstr. 39, Berlin 10117, Germany.
E-Mail: hutt@wias-berlin.de

A stability analysis is presented for neural field equations in the presence of axonal delays and for a general class of connectivity kernels and synaptic properties. Sufficient conditions are given for the stability of equilibrium solutions. It is shown that the delays play a crucial role in non-stationary bifurcations of equilibria, whereas the stationary bifurcations depend only on the kernel. Bounds are determined for the frequencies of bifurcating periodic solutions. A perturbative scheme is used to calculate the types of bifurcations leading to spatial patterns, oscillatory solutions, and traveling waves. For high transmission speeds a simple method is derived that allows the determination of the bifurcation type by visual inspection of the Fourier transforms of the connectivity kernel and its first moment. Results are numerically illustrated on a class of neurologically plausible second order systems with combinations of Gaussian excitatory and inhibitory connections.

*Supported by DFG Research Center "Mathematics for key technologies:" (FZT86) in Berlin, Germany

# 1 Introduction

In recent years, there has been growing interest in the mechanisms of spatio-temporal activity in neural tissue. In this line, applications of various experimental techniques [28, 15, 30, 32] revealed formations of different spatial patterns, traveling waves and pulses[19, 34, 39], standing pulses (e.g. [12]) or irregular spatial patterns [2, 31]. Since neural tissue exhibits multi-scale properties in space and time, the analysis of such activity represents a challenging task. However, reduced biological models at fixed scales in time and space simplify the analysis and allows for analytical treatments (see e.g. [4, 8, 33] for review). In this context, a well-known approach is to focus on neuronal ensembles [37, 38, 20], which allows for the succesful reconstruction of empirical data measured on a macroscopic scale [17, 21, 26, 25, 18].

On a small spatial level ($\sim 50\mu m$), model neurons may consists of two compartments: synapses, which convert incoming action potentials to postsynaptic potentials, and a trigger zone, where these potentials sum up and are re-converted to outgoing action potentials. Due to the large spatial density of neurons ($\sim 10^4$ neurons$/mm^3$), one might consider ensemble activity on a larger spatial scale ($> 1mm$), obtaining a coarse-grained description in space and time [37]. Consequently, macroscopic state variables of neuronal ensembles are mean pulse rates $P(x,t)$ and mean postsynaptic potentials $\Psi(x,t)$. In the following, all measures are meant to represent means of microscopic measures.

Since the link between the microscopic description and the level of neural ensembles has been established in several previous works (e.g. [37, 29, 4, 3]), we only briefly outline the basic mechanisms of activity conversion in neuronal fields. At chemical passive synapses, incoming pulse activity $J(x,t)$ is converted to postsynaptic potentials by convolution with an impulse response function $h(t)$, yielding

$$\Psi(x,t) = \int_{-\infty}^{t} h(t-\tau) J(x,\tau) d\tau.$$

Since neuronal fields exhibit non-local interactions via axonal connections between synapses, incoming pulse activity obeys

$$J(x,t) = \beta \int_{\Omega} K(x,y) P(y, t - \Delta(x,y)) dy \; + \; E(x,t),$$

where $\Omega$ is an appropriate spatial domain, $K(x,y)$ is the connectivity kernel, $\beta > 0$ is a scaling factor and $E$ is an additional external input. In the case of

undamped axonal pulse propagation with finite velocity $v$ and no additional constant delay, we get $\Delta(x,y) = |x-y|/v$. Essentially, the chain of activity conversion closes by the conversion of postsynaptic potentials to pulse rates

$$P(x,t) = S[\Psi(x,t)],$$

where $S$ is called the transfer function. Considering all conversions, we obtain the integral equation

$$\Psi(x,t) = \int_{-\infty}^{t} d\tau \int_{\Omega} dy\ h(t-\tau)K(x,y)S[\Psi(y,\tau-|x-y|/v)] + E(x,\tau).$$

Finally, we recast the impulse response function as a Green's function and thus stipulate

$$\hat{L}h(t) = \delta(t)$$

introducing a temporal differential operator $\hat{L}$. Hence, the final equation reads

$$L(\partial/\partial t)V(x,t) = \beta \int_{\Omega} K(x-y)S(V(y,t-|x-y|/v))\,dy + E(x,t). \quad (1)$$

Here $L$ is a polynomial and $L(\partial/\partial t)$ denotes a temporal differentiation operator with constant coefficients. It is assumed that $L$ is a stable polynomial, i.e., all its roots have negative real parts. We shall refer to (1) as an $n$-th order system where $n \geq 1$ is the order of $L$. The kernel $K : \mathbf{R} \to \mathbf{R}$ is continuous, integrable, and even, that is, $K(-z) = K(z)$ for all $z \in \mathbf{R}$. The transfer function $S : \mathbf{R} \to \mathbf{R}$ is assumed to be differentiable and monotone increasing; in most works it is taken to have a sigmoidal shape.

The model (1) has been treated in the literature in several contexts and with different choices for $L$. In most studies the effect of transmission speed has been neglected by letting $v = \infty$ in the model, the justification being that the signal propagation is sufficiently fast or the spatial scales of the problem are small [23]. Some recent works [4, 10, 13, 22, 16, 6] have addressed the case of finite $v$ by numerical investigations for particular choices of the kernel $K$. Our aim is to give an analytical treatment of the effects of finite transmission speeds for general $K$ and $L$.

## 2 Stability of equilibrium solutions

It is often convenient to normalize the time and space in (1). For instance, if $l$ and $\tau$ are some characteristic length and time of the physical problem, then one can define $\bar{t} = t/\tau$, $\bar{x} = x/l$, $\bar{V}(\bar{x}, \bar{t}) = V(l\bar{x}, \tau\bar{t})$, $\bar{E}(\bar{x}, \bar{t}) = E(l\bar{x}, \tau\bar{t})$, $\bar{L}(\partial/\partial\bar{t}) = \tau^n L(\tau^{-1}\partial/\partial\bar{t})$, $\bar{K}(\bar{z}) = K(l\bar{z})$, and $\bar{v} = \tau v/l$ so that (1) becomes

$$\bar{L}(\partial/\partial\bar{t})\bar{V}(\bar{x}, \bar{t}) = l\tau^n\beta \int_\Omega \bar{K}(\bar{x} - \bar{y})S(\bar{V}(\bar{y}, \bar{t} - |\bar{x} - \bar{y}|/\bar{v}))\, d\bar{y} + \bar{E}(\bar{x}, \bar{t})$$

which has the same form as (1). A common choice for characteristic time is $\tau^n = 1/L(0)$, in which case $\bar{L}(0) = 1$. Thus without loss of generality we consider (1) with the assumption that $L(0) = 1$. Most studies of neuronal fields assume first or second order time derivatives in (1). To address these models in a unified manner we shall often refer to the following specific form

$$L(\lambda) = \eta\lambda^2 + \gamma\lambda + 1, \quad \eta = 0 \text{ or } 1,\ \gamma > 0 \tag{2}$$

although certain results will be stated for arbitrary order stable polynomials $L$. For the spatial domain we assume $\Omega = \mathbf{R}$; but all the results remain valid virtually without modification when $\Omega$ is a circle.

For a constant input $E(x, t) \equiv E^*$, an equilibrium solution $V(x, t) \equiv V^*$ satisfies

$$V^* = \beta \int_{-\infty}^{\infty} K(x - y)S(V^*)\, dy + E^*. \tag{3}$$

Let

$$\kappa = \int_{-\infty}^{\infty} K(z)\, dz = 2\int_0^{\infty} K(z)\, dz. \tag{4}$$

Then (3) can be written as

$$f(V^*) \stackrel{\text{def}}{=} V^* - \kappa\beta S(V^*) = E^*. \tag{5}$$

If $S$ is bounded then $f : \mathbf{R} \to \mathbf{R}$ is surjective; thus (5) has a solution $V^*$ for any $E^* \in \mathbf{R}$. The uniqueness of $V^*$ depends on the sign of $\kappa$ and the shape of $S$. If $S$ is positive and increasing on $\mathbf{R}$, such as a sigmoid function, and if $\kappa \le 0$, then $f$ is increasing and hence also injective, in which case the solution $V^*$ is unique. On the other hand if $\kappa > 0$ then there may be multiple equilibria, as (5) can have more than one solution $V^*$ for a given $E^*$.

The stability of the equilibrium solution $V^*$ is determined by the linear variational equation

$$L(\partial/\partial t)u(x,t) = \alpha \int_{-\infty}^{\infty} K(x-y)u(y, t-|x-y|/v)\, dy \tag{6}$$

where $u(x,t) = V(x,t) - V^*$ and $\alpha = \beta S'(V^*) > 0$. We shall use $\alpha$ as a bifurcation parameter in the following sections. Using the ansatz $u(x,t) = e^{\lambda t}\varphi(x)$ in (6) one obtains

$$L(\lambda)\varphi(x) = \alpha \int_{-\infty}^{\infty} K(x-y) \exp(-\lambda|x-y|/v)\varphi(y)\, dy. \tag{7}$$

Thus $\varphi$ is an eigenfunction of an integral operator. Due to the difference kernel the eigenfunctions have the form $\varphi(x) = e^{ikx}$ for some $k \in \mathbf{R}$, and substituting into (7) followed by a change of variables $z = x - y$ in the integral gives

$$L(\lambda) = \alpha \int_{-\infty}^{\infty} K(z) \exp(-\lambda|z|/v) \exp(-ikz)\, dz. \tag{8}$$

The integral above is the Fourier transform of the function $K_\lambda(z) = K(z)\exp(-\lambda|z|/v)$ (up to a multiplicative factor depending on which definition one uses), which is also equal to its cosine transform since $K_\lambda(z)$ is an even function of $z$. The dispersion relation (8) between the temporal and spatial modes $\lambda$ and $k$ is in general difficult to solve explicitly. A notable exception is the case of instantaneous information transmission, since when $v = \infty$ the right hand side of (8) is independent of $\lambda$. In this paper we shall be interested in finite transmission speeds.

The solutions $(\lambda, k)$ of (8) correspond to the perturbations $u(x,t) = e^{\lambda t}e^{ikx}$ about the equilibrium solution, which grow or decay in time depending on whether $\operatorname{Re}\lambda$ is positive or negative, respectively, thus determining the stability of $V^*$. We give sufficient conditions for asymptotic stability.

**Theorem 1** *Let $c = \alpha \int_{-\infty}^{\infty} |K(z)|\, dz$. If*

$$c < \min_{\omega} |L(i\omega)| \tag{9}$$

*then $V^*$ is asymptotically stable. In particular, if $L(\lambda) = \lambda + 1$ then the condition*

$$c < 1 \tag{10}$$

*is sufficient for the asymptotic stability of* $V^*$. *If* $L(\gamma) = \lambda^2 + \gamma\lambda + 1$ *with* $\gamma > 0$, *then* $V^*$ *is asymptotically stable provided that the condition*

$$\frac{\gamma^2}{2} > 1 - \sqrt{1 - c^2} \tag{11}$$

*holds in addition to (10).*

The following lemma will be useful in the proof of the theorem.

**Lemma 1** *Let* $L(\lambda)$ *be a polynomial whose roots have nonpositive real parts. Then*

$$|L(\sigma + i\omega)| \geq |L(i\omega)|$$

*for all* $\sigma \geq 0$ *and* $\omega \in \mathbf{R}$.

**Proof.** If $\lambda_k$ denote the roots of $L$, then $L(\lambda) = (\lambda - \lambda_1)(\lambda - \lambda_2)\cdots(\lambda - \lambda_n)$, where $n$ is the order of $L$. Thus

$$\begin{aligned} |L(\sigma + i\omega)| &= \prod_{k=1}^{n} |\sigma + i\omega - \lambda_k| \\ &= \prod_{k=1}^{n} \left((\sigma - \operatorname{Re}[\lambda_k])^2 + (\omega - \operatorname{Im}[\lambda_k])^2\right)^{1/2}. \end{aligned}$$

By assumption, $\sigma \geq 0$ and $\operatorname{Re}[\lambda_k] \leq 0$ for all $k$, so

$$\begin{aligned} |L(\sigma + i\omega)| &\geq \prod_{k=1}^{n} \left((-\operatorname{Re}[\lambda_k])^2 + (\omega - \operatorname{Im}[\lambda_k])^2\right)^{1/2} \\ &= \prod_{k=1}^{n} |i\omega - \lambda_k| \\ &= |L(i\omega)|. \end{aligned}$$

■

*Proof of Theorem 1.* In the ansatz $u(x,t) = e^{\lambda t}e^{ikx}$ let $\lambda = \sigma + \mathrm{i}\omega$ where $\sigma$ and $\omega$ are real numbers. We will prove that $\sigma < 0$ if (9) holds. Suppose by

way of contradiction that (9) holds but $\sigma \geq 0$. ¿From the dispersion relation (8) it follows that

$$\begin{aligned} |L(\sigma + i\omega)| &= \alpha \left| \int_{-\infty}^{\infty} K(z) \exp(-(\sigma + i\omega)|z|/v) \exp(-ikz)\, dz \right| \\ &\leq \alpha \int_{-\infty}^{\infty} |K(z)|\, |\exp(-(\sigma + i\omega)|z|/v)|\, dz \\ &\leq \alpha \int_{-\infty}^{\infty} |K(z)| dz = c. \end{aligned} \tag{12}$$

On the other hand, by Lemma 1,

$$|L(i\omega)| \leq |L(\sigma + i\omega)|,$$

which together with (12) implies

$$|L(i\omega)| \leq c$$

for some $\omega \in \mathbf{R}$. This, however, contradicts (9). Thus $\sigma < 0$, and the equilibrium solution is asymptotically stable. This proves the first statement of the theorem. In the specific case when $L$ is given by $L(\lambda) = \lambda + 1$, one has $|L(i\omega)|^2 = 1 + \omega^2$. Hence if (10) is satisfied, then

$$c^2 < 1 \leq 1 + \omega^2 = |L(i\omega)|^2 \quad \text{for all } \omega \in \mathbf{R}$$

which is a sufficient condition for stability by (9). Similarly, suppose $L$ has the form $L(\lambda) = \lambda^2 + \gamma\lambda + 1$ and suppose that (10) and (11) are satisfied. Then

$$|L(i\omega)|^2 = (1 - \omega^2)^2 + (\gamma\omega)^2.$$

Consider now the function

$$\begin{aligned} g(\omega) &\stackrel{\text{def}}{=} |L(i\omega)|^2 - c^2 \\ &= \omega^4 + (\gamma^2 - 2)\omega^2 + (1 - c^2). \end{aligned} \tag{13}$$

If $\gamma^2 \geq 2$ then $g(\omega)$ is positive for all $\omega$ by (10). On the other hand if $\gamma^2 < 2$, then by (11)

$$0 < 2 - \gamma^2 < 2\sqrt{1 - c^2}$$

implying that the discriminant $(\gamma^2 - 2)^2 - 4(1 - c^2)$ is negative; so $g$ has no real roots. Thus in either case $g(\omega)$ is positive, or equivalently $c < |L(i\omega)|$, for all $\omega$, and stability again follows by the first statement of the theorem. ■

# 3 Bifurcations

When $\alpha = 0$, the eigenvalues $\lambda$ are simply given by the roots of $L$, so that $\operatorname{Re}\lambda < 0$ by the assumption that $L$ is a stable polynomial, and the equilibrium point is asymptotically stable. As $\alpha$ is increased, stability may be lost if an eigenvalue $\lambda$ crosses the imaginary axis, and a dynamically different behavior may result in the original nonlinear equation (1). At the critical transition there is an eigenvalue of the form $\lambda = i\omega$, $\omega \in \mathbf{R}$, and the dispersion relation (8) becomes

$$L(i\omega) = \alpha \int_{-\infty}^{\infty} K(z) \exp(-i(kz + \omega|z|/v))\, dz. \tag{14}$$

The possibilities for the resulting behavior when $\alpha$ is near such a critical value can then be qualitatively classified as follows:

I. Stationary bifurcations

   (a) $\omega = 0$ and $k = 0$ : bifurcation to a spatially and temporally constant solution.

   (b) $\omega = 0$ and $k \neq 0$ : bifurcation to a spatially periodic solution which is constant in time, leading to spatial patterns (Turing modes).

II. Non-stationary bifurcations

   (a) $\omega \neq 0$ and $k = 0$ : Hopf bifurcation to periodic oscillations of a spatially uniform solution.

   (b) $\omega \neq 0$ and $k \neq 0$ : bifurcation to traveling waves, with wave speed equal to $\omega/k$.

The conditions for stationary bifurcations are easily characterized by the relation (14) recalling the assumption that $L(0) = 1$. Thus for Case Ia one has

$$1 = \alpha \int_{-\infty}^{\infty} K(z)\, dz = \alpha\kappa \tag{15}$$

with $\kappa$ as defined in (4). This is only possible if $\kappa > 0$, and is the mechanism for appearance of multiple equilibrium solutions of (3). Similarly, the condition (8) for Case Ib is

$$1 = \alpha \int_{-\infty}^{\infty} K(z) \exp(ikz)\, dz = \alpha\hat{K}(k), \quad k \neq 0, \tag{16}$$

where $\hat{K}$ denotes the Fourier transform of $K$. As $\alpha$ is increased from zero, the first mode that becomes unstable in the linearized equation is expected to give an indication of what would be observed in the full nonlinear system (1). Hence, spatial patterns are typically observed as bifurcations from equilibria if a nonzero $k$ is the first mode that loses stability. From (16) it follows that a necessary condition for this is that the maximum value of the Fourier transform of $K$ is positive and occurs at a nonzero frequency $k$.

It is clear from (15) and (16) that stationary bifurcations are independent of the order of the temporal differentiation operator $L$ or the transmission speed $v$. Their analysis only involves the properties of the Fourier transform of the kernel function. On the other hand, $L$ and $v$ turn out to be crucial in non-stationary bifurcations, which will be our main focus in the remainder of the paper. Indeed, our next result shows that a sufficiently small transmission speed is actually a necessary condition for non-stationary bifurcations in first and second order systems.

**Proposition 2** *Suppose $L(\lambda) = \eta\lambda^2 + \gamma\lambda + 1$ with $\gamma > 0$ ($\eta$ may possibly be zero). If*

$$v > \frac{\alpha}{|\gamma|} \int_{-\infty}^{\infty} |zK(z)|\, dz \tag{17}$$

*then (6) has no solutions of the form $u(x,t) = \exp i(\omega t + kx)$ with $\omega$ real and nonzero.*

**Proof.** ¿From the dispersion relation (8),

$$\begin{aligned} L(\lambda) &= \alpha \int_{-\infty}^{\infty} K(z) \exp(-\lambda|z|/v)(\cos kz - i \sin kz)\, dz \\ &= \alpha \int_{-\infty}^{\infty} K(z) \exp(-\lambda|z|/v) \cos kz\, dz \end{aligned}$$

since the function $K(z)\exp(-\lambda|z|/v)$ is even in $z$. Separating the real and imaginary parts of the above expression at the bifurcation value $\lambda = i\omega$ gives

$$\operatorname{Re} L(i\omega) = \alpha \int_{-\infty}^{\infty} K(z) \cos(\omega z/v) \cos(kz)\, dz \tag{18}$$

$$\operatorname{Im} L(i\omega) = -\alpha \int_{-\infty}^{\infty} K(z) \sin(\omega|z|/v) \cos(kz)\, dz \tag{19}$$

Suppose $L(\lambda) = \eta\lambda^2 + \gamma\lambda + 1$. Then $\operatorname{Im} L(i\omega) = \gamma\omega$, and (19) implies

$$\begin{aligned} |\gamma\omega| &= \alpha \left| \int_{-\infty}^{\infty} K(z) \sin(\omega|z|/v) \cos(kz)\, dz \right| \\ &\leq \alpha \int_{-\infty}^{\infty} |K(z) \sin(\omega z/v)|\, dz \\ &\leq \alpha \int_{-\infty}^{\infty} |K(z)\omega z/v|\, dz \end{aligned}$$

where we have used the estimate $|\sin(x)| \leq |x|$ for all $x \in \mathbf{R}$. If $\omega \neq 0$, then $|\omega|$ may be cancelled in the last inequality to yield

$$|\gamma| \leq \frac{\alpha}{v} \int_{-\infty}^{\infty} |zK(z)|\, dz.$$

This, however, contradicts the assumption (17). Hence $\omega = 0$, which proves the proposition. ■

We note that in third and higher order systems bifurcation values $\lambda = i\omega \neq 0$ may occur even with $v = \infty$.

In systems of all orders, it is possible to put *a priori* bounds on the possible values of $\omega$ in terms of the kernel function, as given by the next result.

**Proposition 3** *Let $c$ be as defined in Theorem 1. Then there exists $B > 0$, depending only on $L$ and $c$, such that*

$$|\omega| \leq B \tag{20}$$

*whenever $u(x,t) = \exp i(\omega t + kx)$ is a solution of (6). Furthermore, if $c < 1$ then there exists $A > 0$, depending only on $L$ and $c$, such that*

$$0 < A \leq |\omega|. \tag{21}$$

*In particular, if $L(\lambda) = \lambda + 1$ then*

$$\omega^2 \leq c^2 - 1, \tag{22}$$

*and if $L(\lambda) = \lambda^2 + \gamma\lambda + 1$ then*

$$\begin{array}{cc} (1 - \frac{1}{2}\gamma^2) - \delta \leq \omega^2 \leq (1 - \frac{1}{2}\gamma^2) + \delta & \text{if} \quad 0 \leq c < 1, \\ 0 \leq \omega^2 \leq (1 - \frac{1}{2}\gamma^2) + \delta & \text{if} \quad c \geq 1 \end{array} \tag{23}$$

*where $\delta = \sqrt{(1 - \frac{1}{2}\gamma^2)^2 - 1 + c^2}$.*

**Remark.** The existence of a solution of the form $u(x,t) = \exp i(\omega t + kx)$ implies that the equilibrium point is not asymptotically stable. It is then a consequence of Theorem 1 that the right sides of the inequalities in (22) and (23) are nonnegative.

**Proof of Proposition 3. .** If $\lambda = i\omega$ satisfies the dispersion relation (8) for some $k$, then

$$|L(i\omega)| \leq \alpha \int_{-\infty}^{\infty} |K(z)|\, dz = c. \tag{24}$$

Since $|L(i\omega)| \to \infty$ as $\omega \to \pm\infty$ for any nonconstant polynomial $L$, the above inequality implies an upper bound $B$ on $|\omega|$, which proves (20). For the particular case when $L(\lambda) = \lambda + 1$, (24) gives

$$|L(i\omega)|^2 = \omega^2 + 1 \leq c^2,$$

proving (22). Similarly, for $L(\lambda) = \lambda^2 + \gamma\lambda + 1$, (24) yields

$$|L(i\omega)|^2 = \omega^4 + (\gamma^2 - 2)\omega^2 + 1 \leq c^2. \tag{25}$$

If we let $u = \omega^2$, then the inequality above is equivalent to saying that possible values of $u \geq 0$ are those which render the function

$$h(u) \stackrel{\text{def}}{=} u^2 + (\gamma^2 - 2)u + (1 - c^2)$$

negative or zero. This is only possible if $h$ has at least one root in the interval $[0, \infty)$, implying that the discriminant $(\gamma^2 - 2)^2 - 4(1 - c^2)$ is nonnegative. Letting $\delta = \sqrt{(1 - \frac{1}{2}\gamma^2)^2 - 1 + c^2}$, the roots of $h$ can be written as $(1 - \frac{1}{2}\gamma^2) \pm \delta$. Thus $h(\omega^2) \leq 0$ for $\omega^2$ satisfying

$$(1 - \tfrac{1}{2}\gamma^2) - \delta \leq \omega^2 \leq (1 - \tfrac{1}{2}\gamma^2) + \delta. \tag{26}$$

It remains to ensure that the interval above is a subset of $[0, \infty)$. If $c < 1$, then both roots of $h$ are nonnegative. For if the smaller root is negative, we have

$$0 > (1 - \tfrac{1}{2}\gamma^2) - \delta > (1 - \tfrac{1}{2}\gamma^2) - |1 - \tfrac{1}{2}\gamma^2|,$$

so $(1 - \frac{1}{2}\gamma^2) < 0$. But then both the conditions (10) and (11) are satisfied, and by Theorem 1 $\lambda = i\omega$ cannot be a solution to (8). On the other hand, if $c \geq 1$, then

$$(1 - \tfrac{1}{2}\gamma^2) - \delta \leq (1 - \tfrac{1}{2}\gamma^2) - |1 - \tfrac{1}{2}\gamma^2| \leq 0$$

and

$$(1 - \tfrac{1}{2}\gamma^2) + \delta \geq (1 - \tfrac{1}{2}\gamma^2) + |1 - \tfrac{1}{2}\gamma^2| \geq 0.$$

So, in this case the lower bound on $\omega^2$ in (26) can be replaced by zero. This establishes (23). Finally, to prove (21) for arbitrary $L$ assume that $c < 1$. Then $1 = L(0) > c$. By the continuity of $L$ there exists $A > 0$ such that $|L(i\omega)| > c$ whenever $|\omega| \leq A$. Since (24) is not satisfied, (6) does not have a solution of the form $\exp i(\omega t + kx)$ with $|\omega| \leq A$, which completes the proof. ■

# 4 Perturbative analysis

In order to study the type of bifurcations that may arise in a give situation, the dispersion relation (14) needs to be solved for $\omega$ and $k$. However, explicit solutions are difficult to obtain for general kernel functions. The results of the previous sections imply that in the absence of delays one has a simpler case, where non-stationary bifurcations do not exist in first and second order systems. It follows that the role of delays can be systematically examined by following the changes in the bifurcation structure as the value of the transmission speed is decreased from infinity. Hence we introduce the parameter $\varepsilon = 1/v$, and consider the change in dynamics as $\varepsilon$ is increased from zero. This leads to an approximation scheme that provides valuable insight into the effects of axonal delays in the dynamics of the system. Consider the power series estimate

$$\exp(-\lambda|z|/v) = \sum_{m=0}^{m=N} \frac{(-\lambda|z|/v)^m}{m!} + \mathcal{O}(v^{-(N+1)}).$$

Substitution in the dispersion relation (8) at the bifurcation value $\lambda = i\omega$ gives a finite series in powers of $\varepsilon = 1/v$,

$$\begin{aligned} L(i\omega) &= \alpha \int_{-\infty}^{\infty} K(z) \exp(-ikz) \left[ \sum_{m=0}^{m=N} \frac{(-i\varepsilon\omega|z|)^m}{m!} + \mathcal{O}(\varepsilon^{N+1}) \right] dz \\ &= \alpha \sum_{m=0}^{m=N} \frac{(-i\varepsilon\omega)^m}{m!} \hat{K}_m(k) + \mathcal{O}(\varepsilon^{N+1}) \end{aligned} \tag{27}$$

where the $\hat{K}_m$ denote the transforms of the moments of $K$:

$$\hat{K}_m(k) = \int_{-\infty}^{\infty} |z|^m K(z) \exp(-ikz)\, dz = 2\int_0^{\infty} z^m K(z) \cos(kz)\, dz. \tag{28}$$

and the integrals are assumed to exist. Separating the real and imaginary parts of (27) then yields

$$\alpha^{-1} \operatorname{Re} L(i\omega) = \hat{K}_0(k) - \frac{\varepsilon^2}{2}\omega^2 \hat{K}_2(k) + \frac{\varepsilon^4}{24}\omega^4 \hat{K}_4(k) - \dots \tag{29}$$

$$\alpha^{-1} \operatorname{Im} L(i\omega) = -\varepsilon\omega \hat{K}_1(k) + \frac{\varepsilon^3}{6}\omega^3 \hat{K}_3(k) - \frac{\varepsilon^5}{120}\omega^5 \hat{K}_5(k) + \dots \tag{30}$$

The number of terms needed for the above series to be useful depends on the value of $\varepsilon$ as well as the shape of the kernel $K$. If $K$ is highly concentrated near the origin then a few terms are sufficient. To make this precise, suppose that $K$ is of exponential order, which is the case in most practical situations. In other words, suppose there exist positive numbers $\kappa_1$ and $\kappa_2$ such that

$$|K(z)| \le \kappa_1 \exp(-\kappa_2 |z|) \quad \text{for all } z \in \mathbf{R}.$$

It then follows from (28) that

$$\begin{aligned} \left|\hat{K}_m(k)\right| &\le \int_{-\infty}^{\infty} |z|^m \kappa_1 \exp(-\kappa_2|z|)\, dz = 2\kappa_1 \int_0^{\infty} z^m \exp(-\kappa_2 z)\, dz \\ &= 2\kappa_1 \kappa_2^{-(m+1)} \Gamma(m+1) = 2\kappa_1 \kappa_2^{-(m+1)} m! \end{aligned}$$

so the $m$-th term in the series (27) is bounded in absolute value by

$$2\frac{\kappa_1}{\kappa_2}\left(\frac{\varepsilon|\omega|}{\kappa_2}\right)^m \le 2\frac{\kappa_1}{\kappa_2}\left(\frac{B}{\kappa_2}\varepsilon\right)^m$$

where we have used Proposition 3 to bound the values of $\omega$. Hence, in case of small $\varepsilon$ (large transmission speed) or $B$ (e.g. small $\alpha$ or $S'$), or a large value of $\kappa_2$ (fast decay of $K$ away from the origin), the finite series has increased accuracy. We assume that at least one of these conditions is satisfied so that a small number of terms suffices to determine the general behavior.

In order to observe the qualitative effects of finite transmission speed, we thus neglect third and higher order terms in $\varepsilon$ in the series (27). Then, for $L$ given by (2), equations (29)-(30) become

$$\alpha^{-1}(1 - \eta\omega^2) = \hat{K}(k) - \tfrac{1}{2}\varepsilon^2\omega^2 \hat{K}_2(k) \tag{31}$$

$$\alpha^{-1}\gamma\omega = -\varepsilon\omega \hat{K}_1(k) \tag{32}$$

where we have substituted the more conventional notation $\hat{K}$ for the Fourier transform $\hat{K}_0$ of the kernel. For stationary bifurcations ($\omega = 0$) one obtains from the first equation that

$$\hat{K}(k) = 1/\alpha \tag{33}$$

which is the same as the conditions (15)-(16) given by exact calculation. For a non-stationary bifurcation $\omega \neq 0$, so (32) implies that

$$\hat{K}_1(k^*) = -\gamma/\varepsilon\alpha. \tag{34}$$

Since $\hat{K}_1$ is continuous and $\hat{K}_1(k) \to 0$ as $k \to \pm\infty$, it has a minimum at some value of $k$, which corresponds to the first mode that loses stability as $\varepsilon$ or $\alpha$ is increased. Thus, let

$$k^* = \min_k \hat{K}_1(k) = \min_k \int_{-\infty}^{\infty} |z| K(z) \exp(-ikz)\, dz, \tag{35}$$

and provided $\hat{K}_1(k^*) < 0$, $k^*$ will be the sought solution of (34). Substituting $k^*$ into (31) gives

$$\omega^2 = \frac{\alpha\hat{K}(k^*) - 1}{\frac{1}{2}\alpha\varepsilon^2\hat{K}_2(k^*) - \eta} \tag{36}$$

which has a solution for $\omega$ whenever the right-hand side is nonnegative. This gives a simple procedure to calculate the pairs $(\omega, k)$ satisfying the dispersion relation and corresponding to the bifurcating solution $\exp(\omega t + kx)$.

It remains to determine what type of bifurcation actually occurs. This depends on the mode by which the equilibrium solution, which is stable for $\alpha = 0$, loses its stability as the bifurcation parameter $\alpha$ is increased. The procedure described in the above paragraph gives a simple graphical method. Thus if one plots the curves $\hat{K}(k)$ and $-\hat{K}_1(k)/\gamma v$ in the same graph, and thinks of $1/\alpha$ as a horizontal line being lowered from $+\infty$, then the first intersection point specifies the bifurcation type. If the horizontal line touches the graph of $\hat{K}(k)$ first, then (33) is satisfied and a stationary bifurcation occurs. If, on the other hand, it touches $-\hat{K}_1(k)/\gamma v$ first, then (34) is satisfied and a non-stationary bifurcation occurs. Furthermore, the value of $k$ at the intersection point being zero or nonzero specifies whether the bifurcating solution is spatially constant or not, respectively. It is worthwhile to note that the the type of bifurcations that can occur depends only the extremal

values of $\hat{K}$ and $\hat{K}_1$ and not on the exact shapes of their graphs. This observation has two important consequences. Firstly, the bifurcation structure depends on some general qualities of the kernel and not on its precise shape. And secondly, although our analysis is based on an approximation scheme, the qualitative conclusions regarding the type of bifurcations are generally robust, except for some degenerate cases such as when the maximum values of $\hat{K}(k)$ and $-\hat{K}_1(k)/\gamma v$ are equal.

An example for the investigation of possible bifurcations is illustrated in Figure 1 for some typical kernel functions representing the possibilities for different types of inhibitory and excitatory interaction within the field. For each kernel type in the first column of the figure, the corresponding graphs of $\hat{K}(k)$ and $-\hat{K}_1(k)/\gamma v$ are plotted in the second column. By the argument outlined above, the possible bifurcations for each type of kernel can be directly read off from the graphs in the second column. The actual graphs in the figure are calculated from Gaussian distributions; however, it is clear that small variations in the graphs do not change the bifurcation types. In this way, it is possible to draw some general conclusions concerning different interaction kernels.

The analysis of presented in this section is useful for having a better understanding about the relationship between the interactions within the field and the resulting dynamical behavior. The Fourier transforms $\hat{K}$ and $\hat{K}_1/\gamma v$ are seen to be crucial in this regard, the former instrumental for stationary bifurcations and the latter the non-stationary ones, for the parameter ranges where the approximation scheme is justified. Outside of this range, e.g. for very low transmission speeds, the higher moments of the kernel are also expected to make contributions to the results. In this case, more terms need to be considered in the series (27), together with a numerical solution of the system (29)-(30). Nevertheless, already in the term $\hat{K}_1/\gamma v$ one can see the ingredients that come into play in creating non-stationary bifurcations, namely the operator $L$ (through $\gamma$) representing the local temporal behavior, the kernel (through $\hat{K}_1$) representing spatial interaction, and the transmission speed connecting the two aspects of the dynamics. Figure 1 gives a summary of the bifurcations resulting from the interplay of these elements. In the next section we present numerical simulations for the corresponding dynamical behavior in the nonlinear system (1), obtained on the basis of the foregoing analysis.

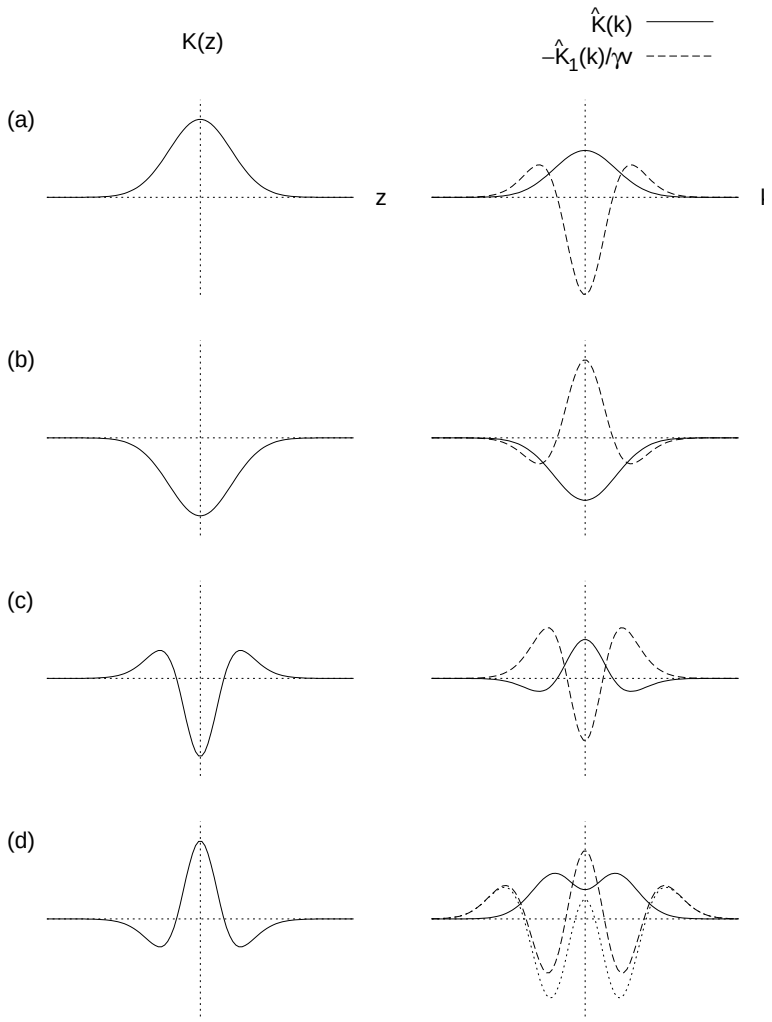


Figure 1: Typical interaction kernels and possible bifurcation types. The first column shows the kernels, with the corresponding Fourier transforms in the second column. The maxima of $\hat{K}$ and $-\hat{K}_1/\gamma v$, respectively, determine the stationary and oscillatory bifurcations, the largest peak giving the actual bifurcation taking place as $\alpha$ is increased. Hence, depending on the value of $\gamma v$, some typical cases are (a) an excitatory field, possible bifurcations Ia and IIb; (b) an inhibitory field, possible bifurcation IIa; (c) local inhibition and lateral excitation, possible bifurcations Ia and IIb; (d) local excitation and lateral inhibition, possible bifurcations Ib and IIa or IIb. In the last subfigure two distinct possibilities for $-\hat{K}_1/\gamma v$ are shown with dashed and dotted lines.

# 5 Applications

We now examine the previous results numerically for a particular model. To this end, we set the differential operator to

$$L(\frac{\partial}{\partial t}) = \frac{\partial^2}{\partial t^2} + \gamma \frac{\partial}{\partial t} + 1, \tag{37}$$

and further specify the connectivity kernel. Since a neuronal field might exhibit excitatory and inhibitory connections, the kernel $K$ contains both excitatory and inhibitory distributions over space. In case of a homogeneous and isotropic neuronal field, a choice of $K$ is

$$K(z) \;=\; \frac{1}{\sqrt{\pi}}(a_e e^{-z^2} - a_i r e^{-r^2 z^2}), \tag{38}$$

where $a_e, a_i$ denote excitatory and inhibitory weights and $r = \sigma_e/\sigma_i$ gives the relation of excitatory and inhibitory spatial connectivity ranges $\sigma_{e,i}$, respectively. In this formulation, the terms in (38) represent probability distributions of excitatory and inhibitory connections, respectively. Thus a purely excitatory connection (Fig. 1a) is obtained when $a_i = 0$ and $a_e > 0$, whereas the choice $a_e = 0$ and $a_i > 0$ gives an inhibitory connection (Fig. 1b). Similarly, for $a_e > a_i > 0$, local inhibition and lateral excitation (Fig. 1c) or local excitation and lateral inhibition (Fig. 1d) can be obtained by choosing $r > a_e/a_i$ or $r < 1$, respectively. We shall mostly focus on these last two cases. Finally, $\beta = 1$ and the transfer function in (1) is chosen to be $S(y) = 1/(1 + \exp(-1.8(y - 3)))$ according to previous works [37, 27].

The subsequent temporal integration procedure applies a fourth-order Runge-Kutta algorithm, while the spatial integration algorithm discretizes the field into $N$ intervals and applies

$$\int_0^L f(z)dz \approx \sum_{i=1}^{N} \frac{1}{2}(f(z_i) + f(z_{i+1}))\Delta x \tag{39}$$

for any function $f$, with $L$ the field length and $\Delta x = L/N$. Further, for periodic boundary conditions, the integration obeys the circular rule

$$\int_{-\infty}^{\infty} K(|x - y|)f(y)dy \approx \int_0^L K(L/2 - |L/2 - |x - y||)f(y)dy. \tag{40}$$

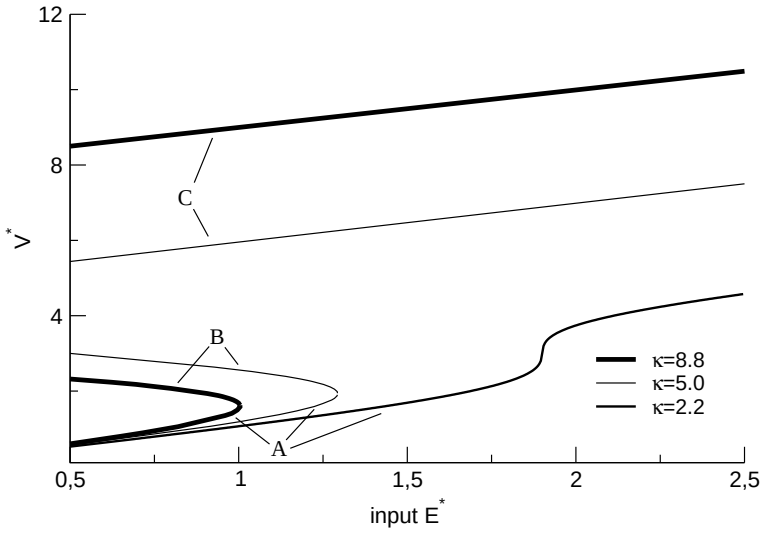


Figure 2: Stationary constant fields $V^*$ plotted with respect to the external input $E^*$ for various parameters $\kappa$. Up to three solutions $A, B, C$ may exist for a given input level.

In subsequent applications we take $N = 400$ and $L = 40$. For integration in space and time initial values

$$V^0(x,t) = V^* + \xi(x,t), \quad -\tau_m \le t \le 0$$

are chosen randomly with the stationary constant state $V^*$ and deviations $\xi(x,t) \in [-0.1; 0.1]$ subject to a uniform distribution. The parameter $\tau_m = L/v$ denotes the maximum temporal delay.

## 5.1 Stability of $V^*$

The equilibria $V^*$ are found from (5). Figure 2 shows solutions $V^*$ of (5) with respect to the external input for various values of $\kappa$. In case $\kappa > 2.2$, there exist up to three solutions A, B, C subject to the external input, whereas there is only a single solution for $\kappa \le 2.2$. Theorem 1 gives a sufficient condition for the stability of these equilibria. Note that for $\gamma > \sqrt{2}$ (11) is automatically satisfied, so $c < 1$ is a sufficient condition for asymptotic stability by Theorem 1. From (38) we have

$$c = \alpha|2a_e\Phi(x_0) - 2a_i\Phi(x_0 r) - (a_e - a_i)|, \quad x_0 = \sqrt{\frac{1}{1-r^2}\ln(\frac{a_e}{a_i r})} \qquad (41)$$

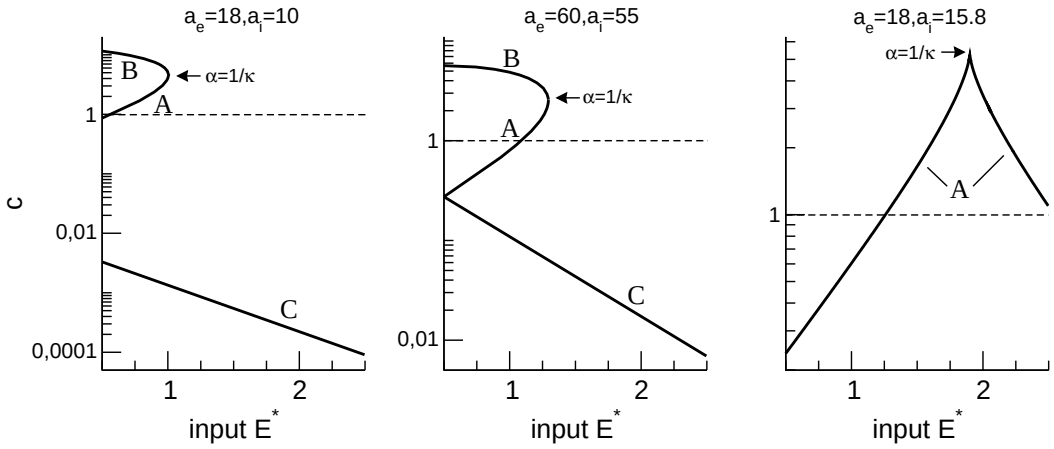


Figure 3: Parameter $c$ from Theorem 1 plotted with respect to the external input $E^*$ for various parameters $a_e, a_i$ and $r = 0.5,\ \gamma > \sqrt{2}$. The characters $A, B$ and $C$ denote stationary solutions (see Fig. 2) and solutions in the region below the dashed line fulfills the sufficient condition of asymptotic stability. It turns out, that stationary solutions $C$ are asymptotically stable for all external inputs in case of $a_e = 18,\ a_i = 10$ and $a_e = 60,\ a_i = 55$.

where $\Phi$ is the Gaussian error function, and $0 < r < 1$ or $r > a_e/a_i$. The spatial distance $x_0$ marks the change of sign of the kernel function and thus separates inhibitory from excitatory connections. The external input $E^*$ affects $c$ through $\alpha = S'(V^*)$. In Fig. 3, $c$ is plotted with respect to the input $E^*$ for $r = 0.5$ and various parameter values of $a_e, a_i$ at the different equilibria $V^*$. Stability is guaranteed by Theorem 1 at least in the region $c < 1$. In this line, Fig. 4 shows a space-time plot of field activity that relaxes to a lower solution $A$ for $c = 0.85$ (cf. Fig. 2). On the other hand, at sufficiently high values of $\alpha$ (and thus of $c$) stability is lost since when

$$\alpha = \frac{1}{\kappa} \tag{42}$$

the condition (15) for a type Ia bifurcation is satisfied. This bifurcaton point is also indicated in Fig. 3. Therefore, the constant solutions denoted $B$ in Figs. 2-3 are unstable. Interestingly, this general result shows accordance to findings in previous works for special connectivity kernels [27, 16]. Finally, in the region $c > 1$ and $\alpha < 1/\kappa$ additional bifurcations might occur yielding loss of stability. These are discussed in the following.

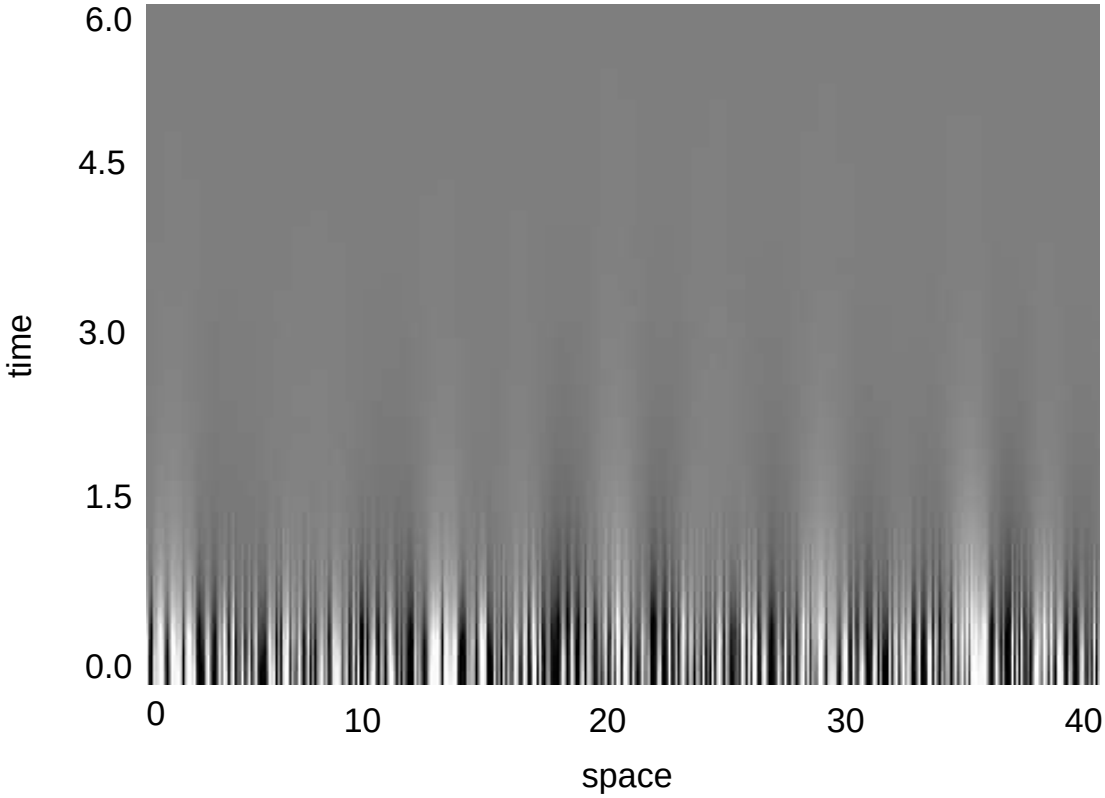


Figure 4: Space-time plot of an asymptotically stable field for the Gaussian connectivity kernel and parameters $E^* = 0.5$, $r = 0.5$, $\gamma = 2$, $a_e = 60$, $a_i = 55$, $v = 100.0$. The grey scale encodes the smooth deviations from the stationary solution, while non-smooth activity results solely from the applied thresholded illustration.

## 5.2 Bifurcations

Recall that the external input defines the set of constant fields $V^*$, which subsequently determine the value of $\alpha$. Hence, $\alpha$ is an appropriate bifurcation parameter. For bifurcations to periodic patterns (Turing case Ib), the threshold condition from Eq. (16) reads

$$\alpha_{thr} = 1/\left(a_e e^{-k_0^2/4} - a_i e^{-k_0^2/4r^2}\right) \quad , \quad k_0^2 = \frac{4r^2}{r^2-1}\ln\frac{a_e r^2}{a_i}, \tag{43}$$

where $k_0 = \arg\max_k \hat{K}(k)$. As $\alpha > 0$, we obtain directly from (43) that $r < 1$, i.e. there is no Turing instability for $r > 1$. Figure 6 displays thresholds $\alpha_{thr}$ with respect to parameters $r$, confirming this finding.

Figure 5 displays a space-time plot of the corresponding Turing instability with $r = 0.5$.

Next, we consider oscillatory phenomena. From Proposition 2, a necessary condition for oscillatory behaviour is

$$v \;<\; v_{thr} = \frac{\alpha}{|\gamma|\sqrt{\pi}}\left[\frac{a_i}{r} - a_e + 2\left(a_e e^{-x_0^2} - \frac{a_i}{r}e^{-r^2x_0^2}\right)\right], \tag{44}$$

with $x_0$ taken from Eq. (41). Figure 7 shows plots of thresholds $v_{thr}$ with respect to the parameter $r$ for two parameter couples of $a_e, a_i$. It turns out that condition (44) is fulfilled and oscillations are expected for a wide range of $r > 1$, whereas $r < 1$ allows only for a small parameter regime.

Further, Section 4 gives conditions for an oscillatory bifurcation in case of large propagation velocity. To obtain oscillating activity constant in space (case IIa), Fig. 1(d) illustrates the conditions $r < 1$ and $-\hat{K}_1(0)/(\gamma v) > \max_k \hat{K}(k)$, implying

$$\frac{a_e - a_i/r}{\gamma v\sqrt{\pi}} > a_e e^{-k_0^2/4} - a_i e^{-k_0^2/4r^2}, \tag{45}$$

where $k_0$ is taken from Eq. (43). Figure 8 displays the corresponding spatio-temporal activity for appropriate parameters.

On the other hand, for traveling waves (case IIb) $k \neq 0$ and Fig. 1(c) gives the conditions $r > a_e/a_i$ and $\max_k -\hat{K}_1(k)/(\gamma v) > \hat{K}(0)$. Using a series expansion for $\hat{K}_1$ [14] we obtain the condition

$$a_e - a_i < \max_k -\frac{1}{\gamma v\sqrt{\pi}}\left(a_e - \frac{a_i}{r} + \sum_{l=1}^{\infty}\left(a_i r^{-2l-1} + a_e\right)\frac{(-1)^{l+1}l!}{(2l)!}k^{2l}\right). \tag{46}$$

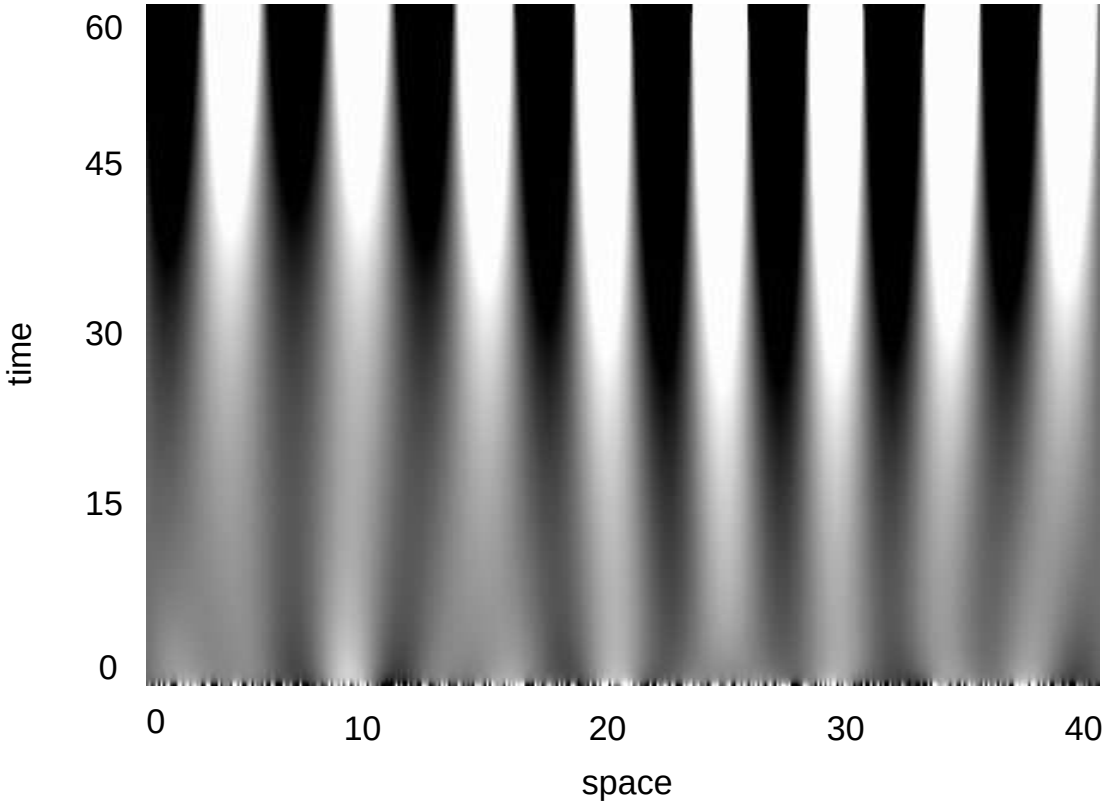


Figure 5: Space-time plot of the Turing instability for the Gaussian connectivity kernel and parameters $E^* = 0.74$, $r = 0.5$, $\gamma = 2$, $a_e = 60$, $a_i = 55$, $v = 100.0$. The grey scale encodes the smooth deviations from the stationary solution, while non-smooth activity results solely from the applied thresholded illustration.

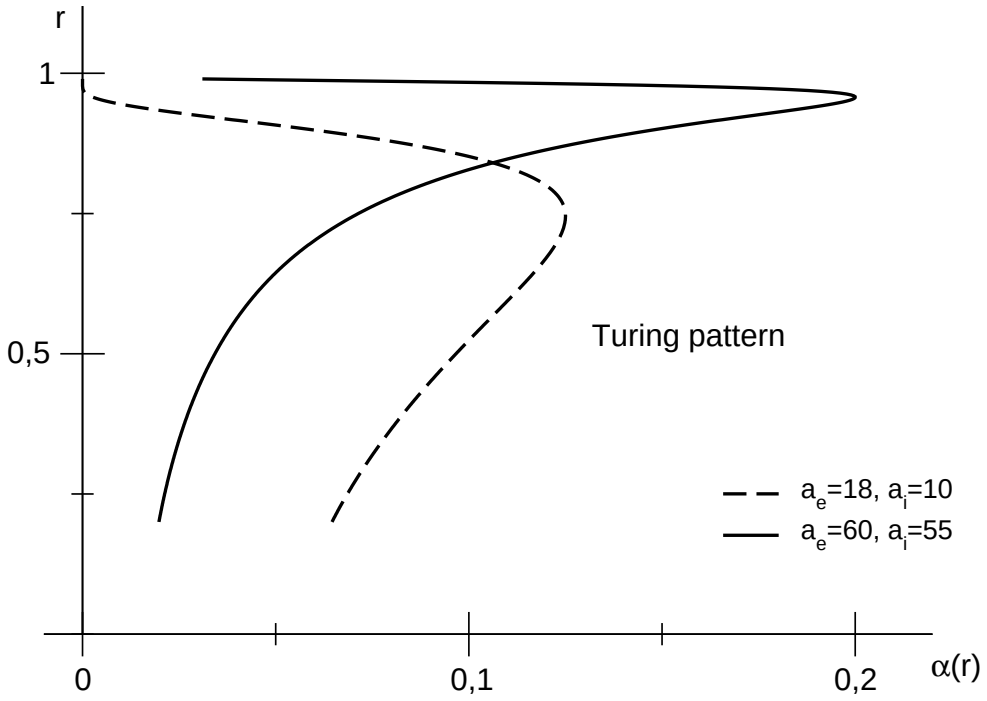


Figure 6: Thresholds of stationary Turing bifurcations $\alpha_{thr}$ plotted for two parameters sets $a_e, a_i$. The regime of the Turing instability obeys $\alpha > \alpha_{thr}$, i.e. the right hand side of each curve.

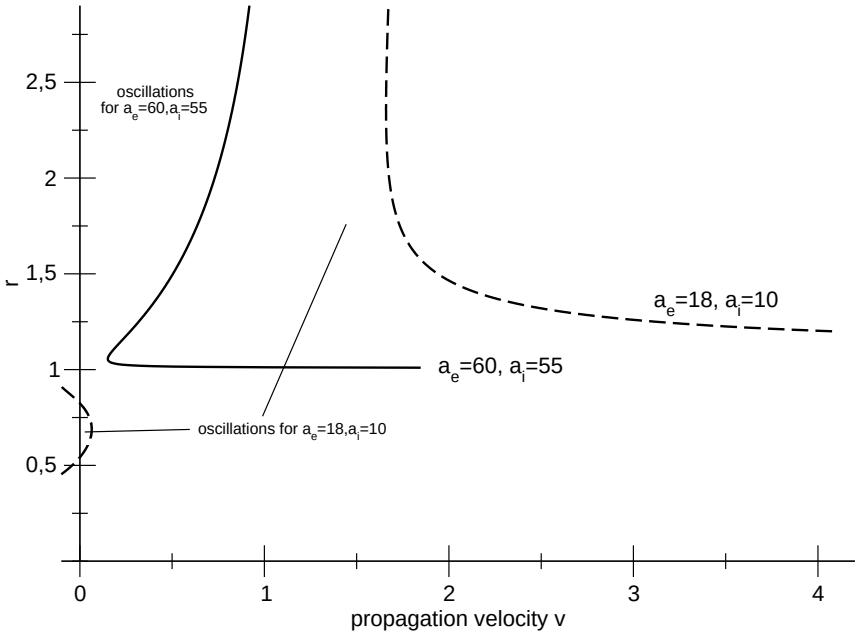


Figure 7: Thresholds of oscillatory phenomena $v_{thr}$ for two parameters sets $a_e, a_i$. The sufficient condition for oscillations is fulfilled for $v < v_{thr}$, i.e. the left hand side of each curve.

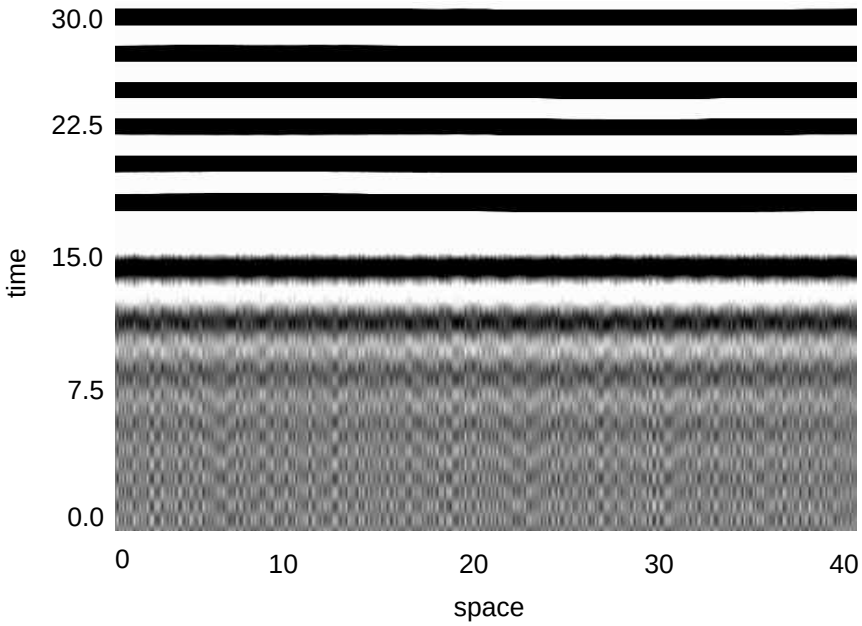


Figure 8: Space-time plot of the Hopf instability for the Gaussian connectivity kernel and parameters $E^* = 0.85$, $r = 0.145$, $\gamma = 0.2$, $a_e = 18$, $a_i = 10$, $v = 8.0$. The grey scale encodes the smooth deviations from the stationary solution, while occuring non-smooth activity results solely from the thresholded illustration.

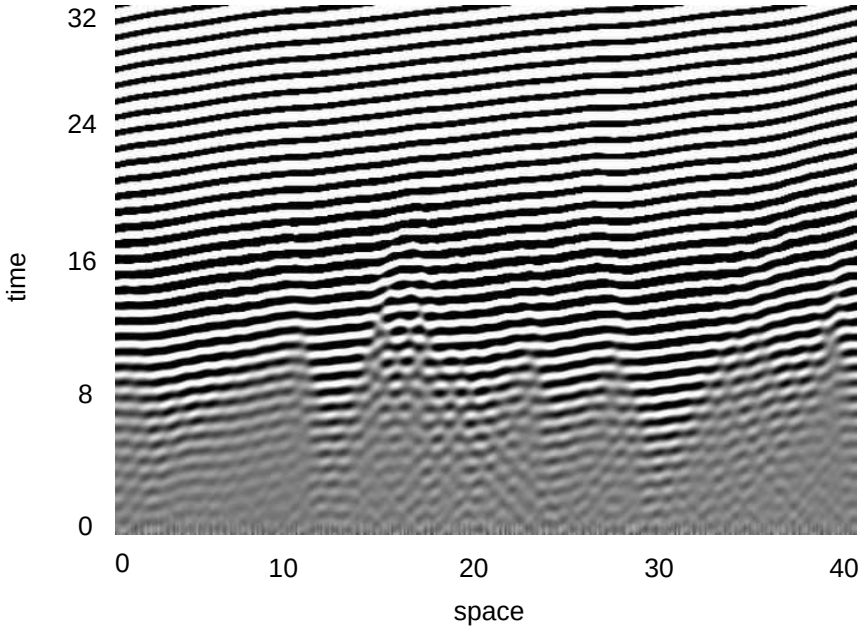


Figure 9: Space-time plot of the wave instability for the Gaussian connectivity kernel and parameters $E^* = 1.29$, $r = 3.0$, $\gamma = 2.0$, $a_e = 60$, $a_i = 55$, $v = 1.0$. The grey scale encodes smooth the deviations from the stationary solution, while non-smooth activity results solely from the applied thresholded illustration.

Figure 9 shows the space-time plot of wave instability for appropriate parameters.

Finally, we examine how the phase velocity of traveling waves depend on the propagation velocity $v$ in the system. From (36) the phase velocity reads

$$v_{ph} = \frac{\omega}{k^*} = \frac{v}{k^*}\sqrt{\frac{\alpha\hat{K}(k^*) - 1}{\frac{1}{2}\alpha\hat{K}_2(k^*) - v^2}}, \tag{47}$$

where $k^*$ solves Eq. (34). In Fig. 10, $v_{ph}$ is plotted and exhibits a slightly nonlinear dependence on the propagation velocity for the applied parameters. We point to the small ratio of phase velocity to propagation velocity in accordance to previous findings [23, 16].

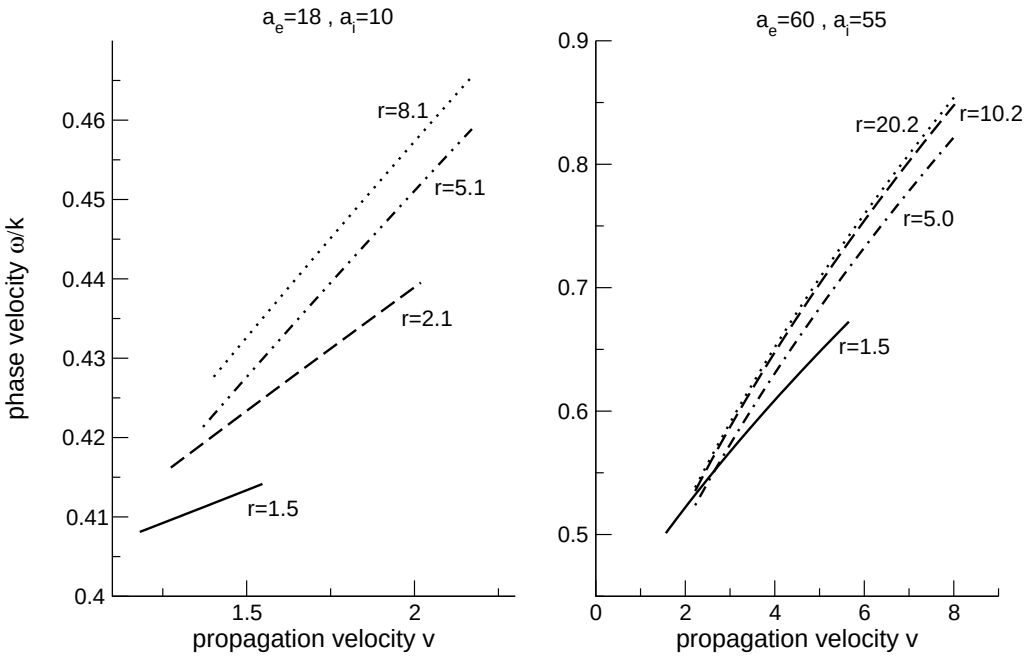


Figure 10: The wave velocity of traveling waves with respect to axonal propagation velocity. Parameters are $\gamma = 0.2$, $0.03 \leq \alpha \leq 0.11$ and $\omega/v \approx 0.7$ (left, for $v \approx 2$) and $\omega/v \approx 0.3$ (right, for $v \approx 7$), respectively.

# 6 Conclusion

We have presented an analysis of the stability of equilibrium solutions for a general class of neural field equations. The details of bifurcations arising from loss of stability provide important information concerning a variety of dynamical behavior that is of neuroscientific interest, including spatial patterns and traveling waves. The stationary bifurcations and the resulting spatial patterns depend only on the connectivity kernel, and are completely determined by its Fourier transform $\hat{K}(k)$. On the other hand, the axonal delays are shown to have significant effects on the non-stationary bifurcations. By a perturbation approach we have characterized these effects in terms of the Fourier transforms of the moments of the kernel function. For high signal transmission speeds, only the first kernel moment needs to be considered to draw qualitative conclusions. This leads to a simple method for determining the possible bifurcation types by comparing the Fourier transforms $\hat{K}(k)$ and $-\hat{K}_1(k)/v\gamma$. Furthermore, the bifurcations depend only on the extremal values of the transforms, rather than the precise shapes of the kernels.

The analysis presented here, being applicable to a broad range of connectivity and synaptic properties and transfer functions, suggests some general conclusions on the types of nonlinear dynamics that can be observed in a fairly wide class of systems. For instance, one generally expects to see oscillatory behavior whenever the signal transmission speed is sufficiently small. In fact, for completely general kernels the peaks of $\hat{K}(k)$ and $-\hat{K}_1(k)$ are more likely to occur at some nonzero $k$ rather than at the precise value $k = 0$. This suggests that the prevalent behavior arising from bifurcations of equilibria will be either spatial patterns or traveling waves, depending on whether the transmission speed is large or small, respectively. Nevertheless, more specific kernel types may dictate different dynamical behavior depending on the application.

Our work is mostly motivated by experimental findings (e.g. [20, 35, 11]). In this line, the presented study aims to generalize the analysis of synaptically-coupled neuronal fields in order to gain a classification scheme for observed spatio-temporal patterns. Here, we would like to mention the important generalization of Amari [1] in lateral-inhibition type fields without axonal delay. Since neurophysiological properties of observed neural tissue are not accessible precisely, a classification scheme might link model functionals with observed phenomena. For example, observed traveling waves necessitate an axonal propagation velocity below a certain threshold defined by

synaptic kernel properties and synaptic response properties (Proposition 2), and furthermore, their frequencies are confined to a bounded band (Proposition 3). In addition, this classification might be important for estimating interaction parameters from multi-site neuronal data (e.g. [9]). Due to the large number of different activity phenomena, further studies in this area could incorporate additional mechanisms like standing and traveling pulse fronts as in [23, 24], boundary effects in local neuronal areas (e.g. [5]), or the influence of external inputs [36, 7] local in space and time.

# References


[1] S. Amari, *Dynamics of pattern formation in lateral-inhibition type neural fields*, Biol. Cybernetics, 27 (1977), pp. 77–87.

[2] G. Blasdel and G. Salama, *Voltage-sensitive dyes reveal a modular organization in monkey striate cortex*, Nature, 321 (1986), pp. 579–585.

[3] P. Bressloff, *Traveling waves and pulses in a one-dimensional network of excitable integrate-and-fire neurons*, J. Math. Biol., 40 (2000), pp. 169–198.

[4] P. Bressloff and S. Coombes, *Physics of the extended neuron*, International Journal of Modern Physics B, 11 (1997), pp. 2343–2392.

[5] C. Cavada and P. S. Goldman-Rakic, *Multiple visual areas in the posterior parietal cortex of primates*, Prog. Brain Res., 95 (1993), pp. 123–137.

[6] S. Coombes, G. Lord, and M. Owen, *Waves and bumps in neuronal networks with axo-dendritic synaptic interactions*, Physica D, 178 (2003), pp. 219–241.

[7] M. Enculescu and M. Bestehorn, *Activity dynamics in nonlocal interacting neural fields*, Phys. Rev. E, 67 (2003), p. 041904.

[8] B. Ermentrout, *Neural networks as spatio-temporal pattern-forming systems*, Reports on Progress in Physics, 61 (1998), pp. 353–430.

[9] O. François, C. Larota, J. Horikawa, and T. Hervé, *Diffusion and innovation rates for multidimensional neuronal data with large spatial covariances*, Network: Comput. Neural Syst., 11 (2000), pp. 211–220.

[10] W. Freeman, *Characteristics of the synchronization of brain activity imposed by finite conduction velocities of axons*, Int. J. Bif. Chaos, 10 (2000), pp. 2307–2322.

[11] ——, *Neurodynamics: An Exploration in Mesoscopic Brain Dynamics (Perspectives in Neural Computing)*, Springer-Verlag, Berlin, 2000.

[12] P. Goldman-Rakic, *Cellular basis of working memory*, Neuron, 14 (1995), pp. 477–485.

[13] D. Golomb and G. Ermentrout, *Effects of delay on the type and velocity of travelling pulses in neuronal networks with spatially decaying connectivity*, Network: Comput. Neural Syst., 11 (2000), pp. 221–246.

[14] I. S. Gradshteyn and I. M. Ryzhik, *Table of Integrals, Series, and Products*, Academic Press, San Diego, 2000.

[15] A. Grindvald, L. Anglister, J. Freeman, R. Hildesheim, and A. Manker, *Real-time optical imaging of naturally evoked electrical activity in intact frog brain*, Nature, 308 (1984), pp. 848–850.

[16] A. Hutt, M. Bestehorn, and T. Wennekers, *Pattern formation in intracortical neuronal fields*, Network: Comput. Neural Syst., 14 (2003), pp. 351–368.

[17] V. Jirsa and H. Haken, *A derivation of a macroscopic field theory of the brain from the quasi-microscopic neural dynamics*, Physica D, 99 (1997), pp. 503–526.

[18] V. Jirsa, K. Jantzen, A. Fuchs, and J. Kelso, *Spatiotemporal forward solution of the EEG and MEG using network modelling*, IEEE Transactions on Medical Imaging, 21 (2002), pp. 493–504.

[19] J. Lance, *Current concepts of migraine pathogenesis*, Neurology, 43 (1993), pp. S11–S15.

[20] P. Nunez, *Neocortical dynamics and human EEG rhythms*, Oxford University Press, New York - Oxford, 1995.

[21] ——, *Toward a quantitative description of large-scale neocortical dynamic function and EEG*, Behav. Brain Sci., 23 (2000), pp. 371–437.

[22] R. Osan and G. Ermentrout, *The evolution of synaptically generated waves in one- and two-dimensional domains*, Physica D, 163 (2002), pp. 217–235.

[23] D. Pinto and G. Ermentrout, *Spatially structured activity in synaptically coupled neuronal networks: I. travelling fronts and pulses*, SIAM J. Applied Math., 62 (2001), pp. 206–225.

[24] ——, *Spatially structured activity in synaptically coupled neuronal networks: II. lateral inhibition and standing pulses*, SIAM J. Applied Math., 62 (2001), pp. 226–243.

[25] C. Rennie, P. Robinson, and J. Wright, *Unified neurophysical model of EEG spectra and evoked potentials*, Biological Cybernetics, 86 (2002), pp. 457–471.

[26] P. Robinson, P. Loxley, S. O'Connor, and C. Rennie, *Modal analysis of corticothalamic dynamics, electroencephalographic spectra and evoked potentials*, Physical Review E, 63 (2001), p. 041909.

[27] P. Robinson, C. Rennie, and J. Wright, *Propagation and stability of waves of electrical activity in the cerebral cortex*, Physical Review E, 56 (1997), pp. 826–840.

[28] B. Salzberg, H. Davila, and L. Cohen, *Optical recording of impulses in individual neurones of an invertebrate central nervous system*, Nature, 246 (1973), pp. 508–509.

[29] H. Schuster and P. Wagner, *A model for neuronal oscillations in the visual cortex: 1. mean-field theory and derivation of the phase equations*, Biol. Cybern., 64 (1990), pp. 77–82.

[30] W. Singer and C. Gray, *Visual feature integration and the temporal correlation hypothesis*, Annual Review Neuroscience, 18 (1995), pp. 555–586.

[31] H. Spors and A. Grindvald, *Spatio-temporal dynamics of odor representations in the mammalian olfactory bulb*, Neuron, 34 (2002), pp. 301–315.

[32] M. Steriade, E. Jones, and R. Llinas, *Thalamic Oscillations and Signalling*, Wiley, New York, 1990.

[33] A. Sturm and P. König, *Mechanisms to synchronize neuronal activity*, Biological Cybernetics, 84 (2001), pp. 153–172.

[34] P. Tass, *Oscillatory cortical activity during visual hallucinations*, J. Biol. Phys., 23 (1997), pp. 21–66.

[35] C. Uhl, ed., *Analysis of Neurophysiological Brain Functioning*, Springer-Verlag, Berlin, 1999.

[36] T. Wennekers, *Dynamic approximation of spatio-temporal receptive fields in nonlinear neural field models*, Neural Computation, 14 (2002), pp. 1801–1825.

[37] H. Wilson and J. Cowan, *A mathematical theory of the functional dynamics of cortical and thalamic nervous tissue*, Kybernetik, 13 (1973), pp. 55–80.

[38] J. Wright and R. Kydd, *The electroencephalogram and cortical neural networks*, Network, 3 (1992), pp. 341–362.

[39] J. Wu, L. Guan, and Y. Tsau, *Propagating activation during oscillations and evoked responses in neocortical slices*, J. Neurosci., 19 (1999), pp. 5005–5015.